J MATER RES TECHNOL. 2019;8(6):5246–5253

Available online at www.sciencedirect.com

jmr&t Journal of Materials Research and Technology

www.jmrt.com.br

Original Article

Corrosion behaviours of hot-extruded Al-xMg alloys

N.D. Nam[a,*], V.D. Phung[a], P.T.P. Thuy[b,c], V.A. Dao[a], S.H. Kim[d], J.S. Yi[d,*]

[a] FM&D Laboratory, Institute of Fundamental and Applied Sciences, Duy Tan University, Ho Chi Minh City 700000, Vietnam
[b] Khanh Hoa Province's Boarding High Schools, 02 Hon Chong Street, Vinh Phuoc Ward, Nha Trang City 650000, Vietnam
[c] Ton Duc Thang University, Nguyen Huu Tho Str., Tan Phong Ward, Dist. 7, Ho Chi Minh City 700000, Vietnam
[d] College of Information and Communication Engineering, Sungkyunkwan University, Suwon 16419, Republic of Korea

ARTICLE INFO

Article history:
Received 31 July 2019
Accepted 26 August 2019
Available online 14 September 2019

Keywords:
Alloys
Extrusion
Grain size
Pitting corrosion
Electrochemistry

ABSTRACT

Aluminum and its alloys have prompted significant development in several industrial fields. However, aluminum is typically very difficult to weld and sometimes generates undesirable formations during various processes. Therefore, the properties of aluminum must be thoroughly investigated to improve its applicability to various engineering problems. In this study, Al-xMg alloys with x = 0, 2, and 4 wt% were successfully formed using a hot extrusion method and characterized using various electrochemical and surface analysis techniques following immersion in a 0.1 M Na_2SO_4 + 0.01 M NaCl solution. The results indicate that an increase in Mg content in Al-based alloys leads to better pitting resistance. This could be a result of significant changes in grain size and passive film formation on alloy surfaces, which lead to superior physical properties.

1. Introduction

Aluminum alloys have played a key role in a wide range of industrial applications based on the desirable mechanical, wear, and corrosion properties of aluminum, as well as its light weight [1,2]. There is a growing interest in wear and corrosion characterizations in terms of both type and quantity in various areas of aluminum alloy technology [3–6]. Therefore, many characterization methods have been applied in many areas [7,8]. Pure aluminum is soft, ductile, and unsuitable for most engineering environments. However, requirements for mechanical strength can be satisfied by the including other alloying elements to increase the strength of aluminum. Two main categories have been defined for aluminum alloys [9,10]: (i) non-heat-treatable aluminum alloys (e.g., alloys containing manganese, silicon, iron, and magnesium) and (ii) heat-treatable aluminum alloys (e.g., alloys containing heavy elements, such as copper and zinc, in addition to magnesium and silicon). Among these alloying elements, silicon is a common element that is added to aluminum alloys to improve castability and machinability based on the presence of hard

* Corresponding authors.
E-mails: nguyendangnam@dtu.edu.vn (N. Nam), junsin@skku.edu (J. Yi).
https://doi.org/10.1016/j.jmrt.2019.08.047

silicon particles [11–13]. However, ductility and machining properties are negatively affected by the formation of faceted and blocky primary Si.

Al-Si alloy series have been a topic of significant interest for a variety of applications based on their homogeneous distributions of eutectic and primary Si particles, which improve mechanical and wear properties [14–16]. However, corrosion evaluations have shown that the dissolution rates of these alloys are significantly influenced by Si content and the characteristics of corrosive environments [17,18]. Pitting corrosion is initially concentrated in areas around primary Si particles based on microgalvanic interactions between cathodic Si content and the anodic Al matrix. The mixture of Al oxide and Si is considered to be a semiconductor that can facilitate the passage of electrons [19], thereby enabling microgalvanic corrosion. Therefore, Si content is the main cause of microgalvanic corrosion in Al-Si alloys [18,20]. Additionally, some heavy metals contained in Al alloys, such as Fe, Cu, Mn, and Zn, can be work and precipitation hardened to increase strength [21–23]. However, uniform distributions of these elements in alloy microstructures can cause localized corrosion based on available microgalvanic cells in α-Al and secondary phases containing heavy metals with inhomogeneous distributions. Furthermore, these series of alloys retain either solute-depleted zones or anodically active phases at grain boundaries, resulting in lower pitting corrosion resistance and breakdown potential, as well as greater vulnerability to stress corrosion cracking and intergranular corrosion [24,25]. The aluminum-magnesium (Al-Mg) series of alloys has become an important class of materials based on its significant advantages in terms of physical and mechanical properties compared to other alloys. It provides good corrosion resistance, a high strength-to-weight ratio, high fatigue strength, good recyclability and cost efficiency, and superior weldability compared to other series of alloys [21,22]. These desirable properties of Al-Mg alloys can be attributed to the effects of Mg content in terms of preventing mobile dislocations [26,27]. Al-Mg series alloys have achieved light weights with good corrosion resistance and mechanical properties based on solid solution strengthening [28–32]. They have seen many structural applications in the automobile, electronics, and aircraft industries based on the improvement of creep strength at high temperatures [33,34]. Based on recent studies, the mechanical strength of aluminum alloys has been successfully enhanced through the use of equal channel angular pressing, extrusion, rolling, and pressure infiltration techniques, as well as the addition of alloying elements [18,35–38]. The addition of 3–6 wt% of magnesium content into Al alloys through continuous rheo-extrusion can eliminate the formation of coarse dendrites and improve mechanical properties [39]. The study above also indicated that ultimate tensile strength increases and elongation decreases with increasing magnesium content. Specifically, the ultimate tensile strength and elongation of an Al-5Mg alloy were improved by 73% and 8%, respectively, compared to those of a conventional casting alloy. Scudino et al. indicated that the strength of an Al alloy containing 5 wt% of Mg fabricated via mechanical alloying is four times greater than that of a conventional Al-5083 alloy with an 8.5% increase ductility [40]. Jeong reported that as the Mg content in an Al-Mg alloy increases from 5 to 7 wt%, the fraction of dynamically recrystallized grains first decreases, then increases, followed by another increase as Mg content increases up to 13 wt% [41]. The study above also indicated that the Al-13Mg alloy provided superior post-deformation microstructures compared to Al-Mg alloys with the lower Mg content. These reports all indicate that adding Mg to aluminum alloys can significantly improve the mechanical properties of such alloys. However, the corrosion resistance of these alloys has not been studied thoroughly. Specifically, no studies have focused on additive components, such as Cl^-, for the retardation of pitting initiation or the incorporation of Cl^- ions into the oxide/hydroxide films (SO_4^{2-}) of aggressive solutions. Therefore, the electrochemical corrosion processes of Al-Mg alloys must be investigated to continue developing and expanding the applications of such alloys. Additionally, high Mg concentrations in Al alloys can lead to intergranular corrosion based on the formation of electrochemically active precipitates, such as supersaturated Al-Mg solid solutions, at grain boundaries [42,43]. Therefore, in this study, we added 0, 2, and 4 wt% of Mg to commercial aluminum alloys to form binary alloys and analyze the effects of alloying elements. Al-xMg alloys were produced using the hot extrusion method and standard electrochemical procedures were applied using solutions containing Cl^- and SO_4^{2-} ions. Surface analysis was also performed.

2. Experiments

Pure Al (0.001% Mg, 0.11% Fe, 0.01% Cr, 0.02% Si, 0.005% Ni) and Mg (0.01% Al, 0.11% Fe, 0.01% Cr, 0.02% Si, 0.005% Ni) ingots were used as starting materials. The calculated amounts of 0, 2, and 4 wt% Mg were then used as alloying element additions. The materials were initially fabricated to appropriate sizes for further processing. They were cleaned via ultrasonication in an acetone solution to remove any contaminants and placed in the crucible of a reaction system. Following solution treatment at 700 °C with a heating rate 10 °C/min in an argon atmosphere and 30 min of mechanical stirring, hot extrusion began with an extrusion ratio of 25:2. Degassing was performed at 500 °C for 5 h and preheating was performed at 450 °C for 1 h while maintaining the die and container temperature at 450 °C. The alloy materials were extruded into specimens with a diameter of 10 mm for further processing. To control the exposed area, these specimen electrodes were coated with a low viscosity epoxy cold mounting system with 17:1 ratio of EpoFix resin and EpoFix hardener curing at room tempera-ture in 12 h, no shrinkage and attached to a Teflon holder. The specimens were then ground using 600-grit silicon carbide sand paper. Additionally, ethanol was used for the grinding process and rinsing the specimens.

Finally, the specimens were ground perpendicularly using different grits of sandpaper until reaching 4000 grit, then polished using 0.5-μm alumina powder prior to electron backscatter diffraction (EBSD) observations. A tilting angle of 70° and a 20-kV camera were used for EBSD measurements via scanning electron microscopy (SEM) using a Zeiss Supra 55 VP microscope. The Supra 55 VP microscope was also used for characterizing surface morphologies following potentiostatic (PS) measurements. Furthermore, the passive layer was char-

acterized using X-ray photoelectron spectroscopy (XPS) with an Al K_α radiation source operating at 1486.6 eV with 15 kV of anodic voltage and 10 mA of anodic current. For these observations, 160 and 20 eV were used for the pass energies of the survey and high-resolution scans, respectively. Additionally, 285.0 eV of the charge for the hydrocarbon C 1s peak were used for calibrating the binding energy.

Next, 1000 ml of 0.1 M Na_2SO_4 + 0.01 M NaCl solution were used for performing electrochemical and coupon immersion experiments under natural aeration. The electrochemical cells, which included alloys, graphite, and a saturated calomel electrode (SCE), were connected to a Biologic VSP system as the working, counter, and reference electrodes, respectively. The open circuit potential (OCP) was monitored for 1 h prior to performing any electrochemical measurements. Electrochemical impedance spectroscopy (EIS) measurements were performed every hour for 14 h with a peak-to-peak amplitude of thesinusoidal perturbation of 10 mV and frequency range of 100 kHz to 10 mHz. For potentiodynamic polarization (PD) tests, a rate of 166×10^{-3} mV/s was used to sweep the potential from −250 mV versus the OCP until reaching the pitting potential. A constant potential of $-550\,mV_{SCE}$ was applied to the working electrode to observe changes in current over time.

3. Results and discussion

To observe alloy microstructures, the alloy specimens were characterized using EBSD after they were polished using 0.5-μm alumina powder. The results are presented in Fig. 1. The EBSD images reveal many defects (black regions) in the Al-based alloy structure in Fig. 1(a). This phenomenon cannot be observed for the Mg-containing alloys, demonstrating the significant effect of Mg on the microstructures of Al-based alloys. The calculated grain size is 0.63 μm for the alloy without Mg, whereas the Mg-containing specimens have relatively small α-Al grains that decrease in size with increasing Mg content (0.63, 0.52, and 0.45 μm for the base alloy, Al-2Mg, and Al-4Mg, respectively). Mg dispersoids may have promoted the development of a passive layer on the Al alloy surfaces. Based on the development of such a layer, the refinement of grain size can significantly affect corrosion properties, highlighting the important role of Mg in the corrosion resistance of Al alloys.

The PD curves for the Al-xMg alloys are presented in Fig. 2(a) and the measured E_{corr} and E_{pit} value are presented in Fig. 2(b). These results indicate that the alloys act as passive materials at a low current density in a 0.1 M Na_2SO_4 + 0.01 M NaCl solution. Furthermore, the ranges of the passive potential and E_{pit} increase significantly as the Mg content in the Al-based alloys increases from 0 to 4 wt%. Therefore, adding Mg to Al-based alloy improves pitting resistance based on increased E_{pit} values and a wider passive potential range. These benefits can be attributed to changes in microstructure and the formation of a stable passive film. These results correlate with the low anodic current densities (less than 0.1 $\mu A/cm^2$) observed in the PS measurements when a constant anodic potential of $-550\,mV_{SCE}$ was applied for 6 h, as shown in Fig. 3. The anodic potential collected in the passivation region corresponds to the PD results in Fig. 2. The PS results indicate that all of the Al-xMg alloys maintain very low current densities when a constant anodic potential of $-550\,mV_{SCE}$ is applied, indicating that the anodic dissolution of these alloys is relatively slow. These results also confirm the stability and durability of the passive film formed on the Al-4Mg surface over 6 h of $-550\,mV_{SCE}$ application. In con-

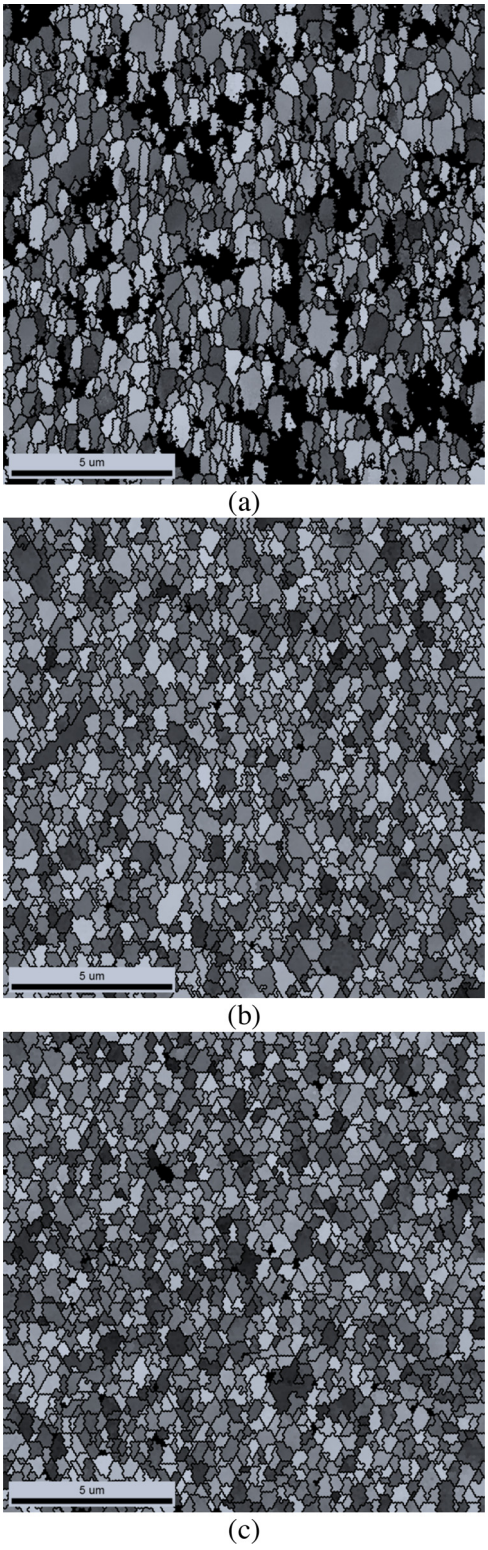

Fig. 1 – EBSD results for (a) pure Al, (b) Al-2Mg and (c) Al-4Mg alloys.

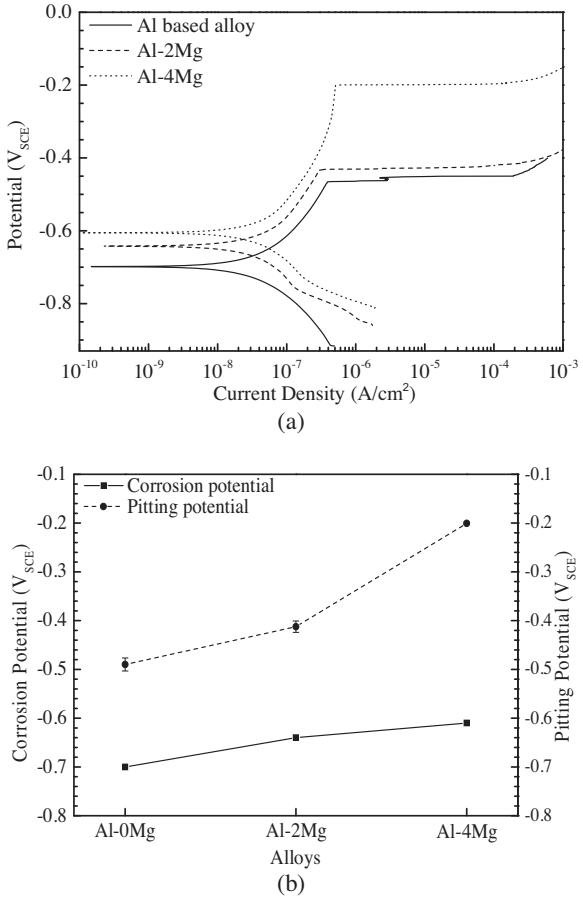

Fig. 2 – (a) Potentiodynamic polarization curves of Al-xMg alloys and (b) effects of Mg on the corrosion and pitting potentials of aluminum alloys in a 0.1 M Na_2SO_4 + 0.01 M NaCl solution.

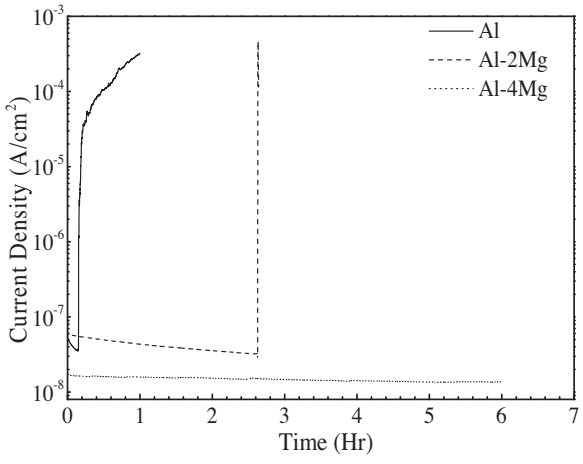

Fig. 3 – Changes in current as a function of time after applying −550 mV_{SCE} to Al-xMg alloys in a 0.1 M Na_2SO_4 + 0.01 M NaCl solution.

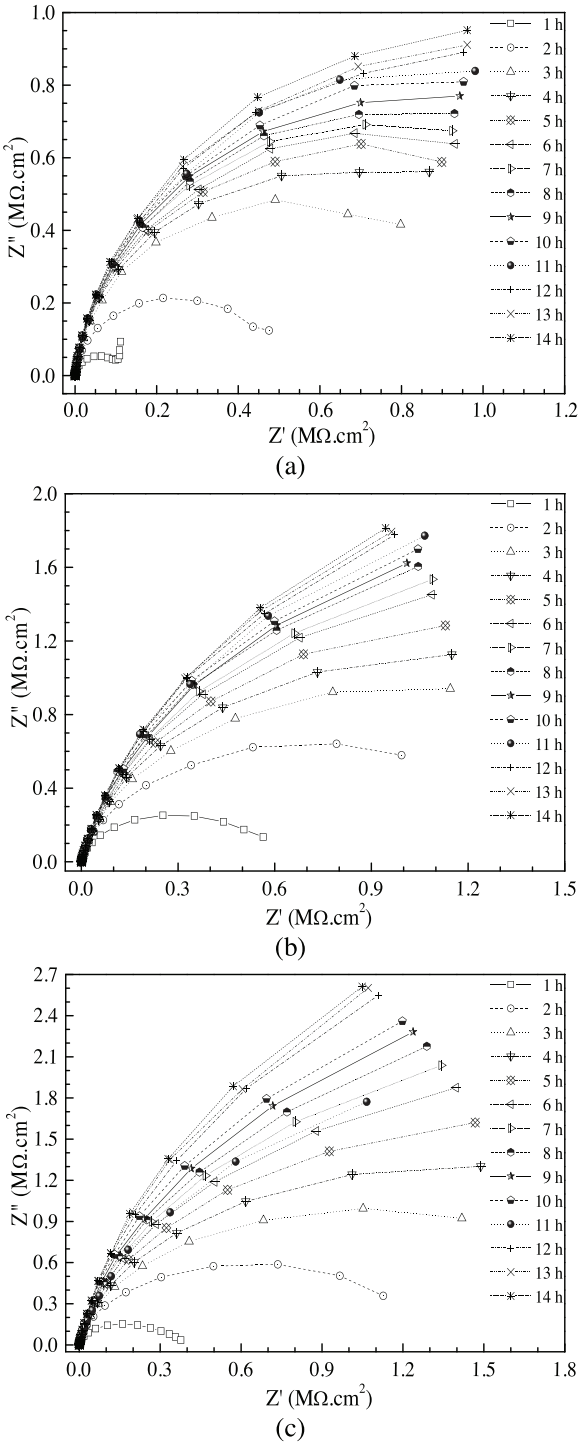

Fig. 4 – Nyquist plots of (a) pure Al, (b) Al-2Mg and (c) Al-4Mg alloys in a 0.1 M Na_2SO_4 + 0.01 M NaCl solution.

trast, the passive films formed on the Al-2Mg alloy and pure Al surfaces break down at 565 and 9443 s, respectively. It can be concluded that the rapid increase in anodic current density is a result of pitting initiation. Therefore, the PS results are consistent with the PD results, indicating evident improvement of the pitting resistance of Al-based alloy when Mg is added as an alloying element.

Fig. 4 presents EIS spectra in the Nyquist form for Al specimens with different Mg contents over 14 h. Heterogeneity of the surfaces may be the reason for the depressed semicircular Nyquist plots in Fig. 4. Furthermore, an increase in arc diameter suggests improved corrosion resistance based on passive

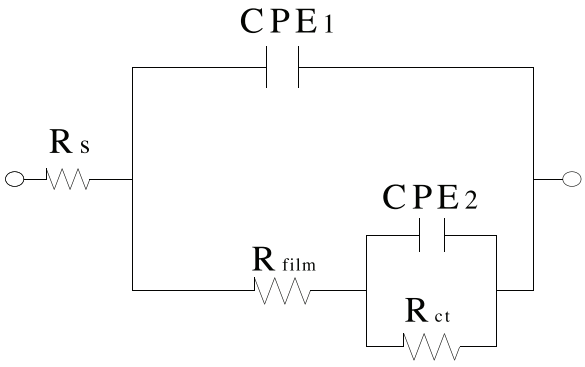

Fig. 5 – Equivalent circuit model for fitting EIS data.

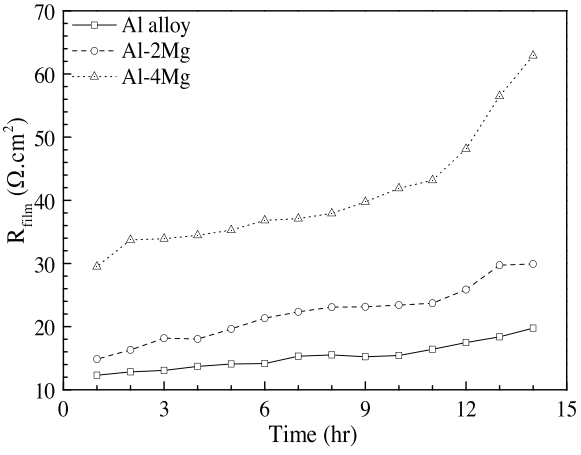

(a)

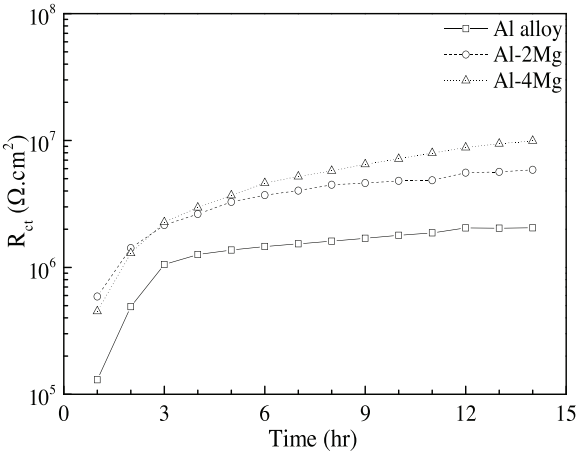

(b)

Fig. 6 – Effects of Mg on the film and charge transfer resistances of Al-xMg alloys in a 0.1 M Na2SO4 + 0.01 M NaCl solution.

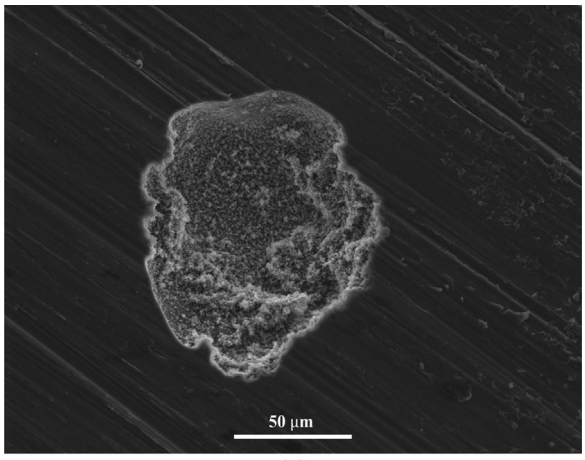

(a)

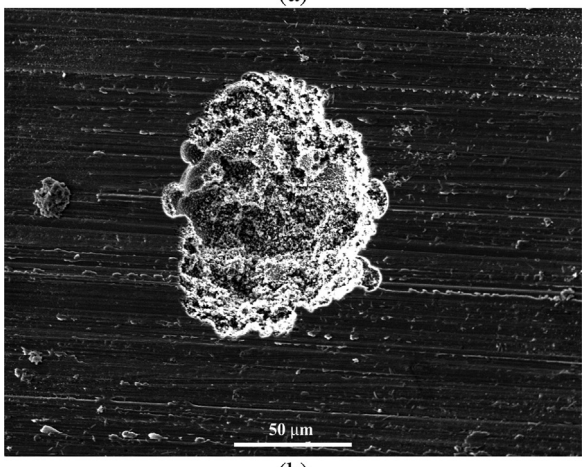

(b)

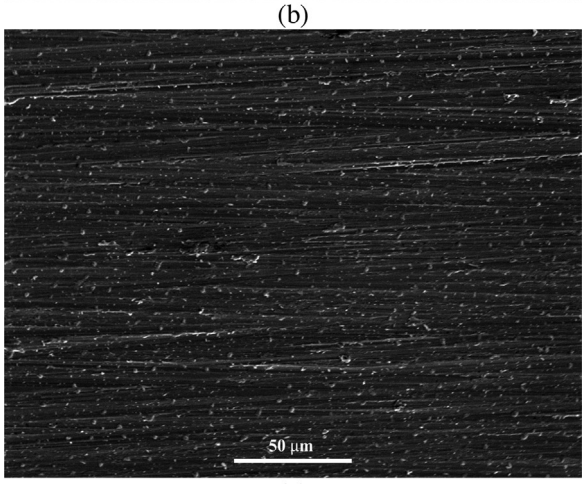

(c)

Fig. 7 – SEM/EDS images of specimens tested after the application of −550 mV$_{SCE}$ and immersion in a 0.1 M Na_2SO_4 + 0.01 M NaCl solution: (a) pure Al, (b) Al-2Mg and (c) Al-4Mg alloys.

film formation. The EIS results also indicate that the addition of Mg to Al-based alloy increases the arc diameter of Nyquist plots as a result of improved pitting resistance. To analyze resistance parameters, a suitable equivalent circuit was constructed to simulate and fit electrochemical responses using the Zsimpwin software. The equivalent circuit in Fig. 5 was chosen for fitting the EIS data for the Al-xMg alloys that formed passive layers on their surfaces when immersed in a naturally aerated 0.1 M Na_2SO_4 + 0.01 M NaCl solution. The equivalent circuit consists of R_s, a constant phase element (CPE) with a capacitance (C) and phenomenological coefficient

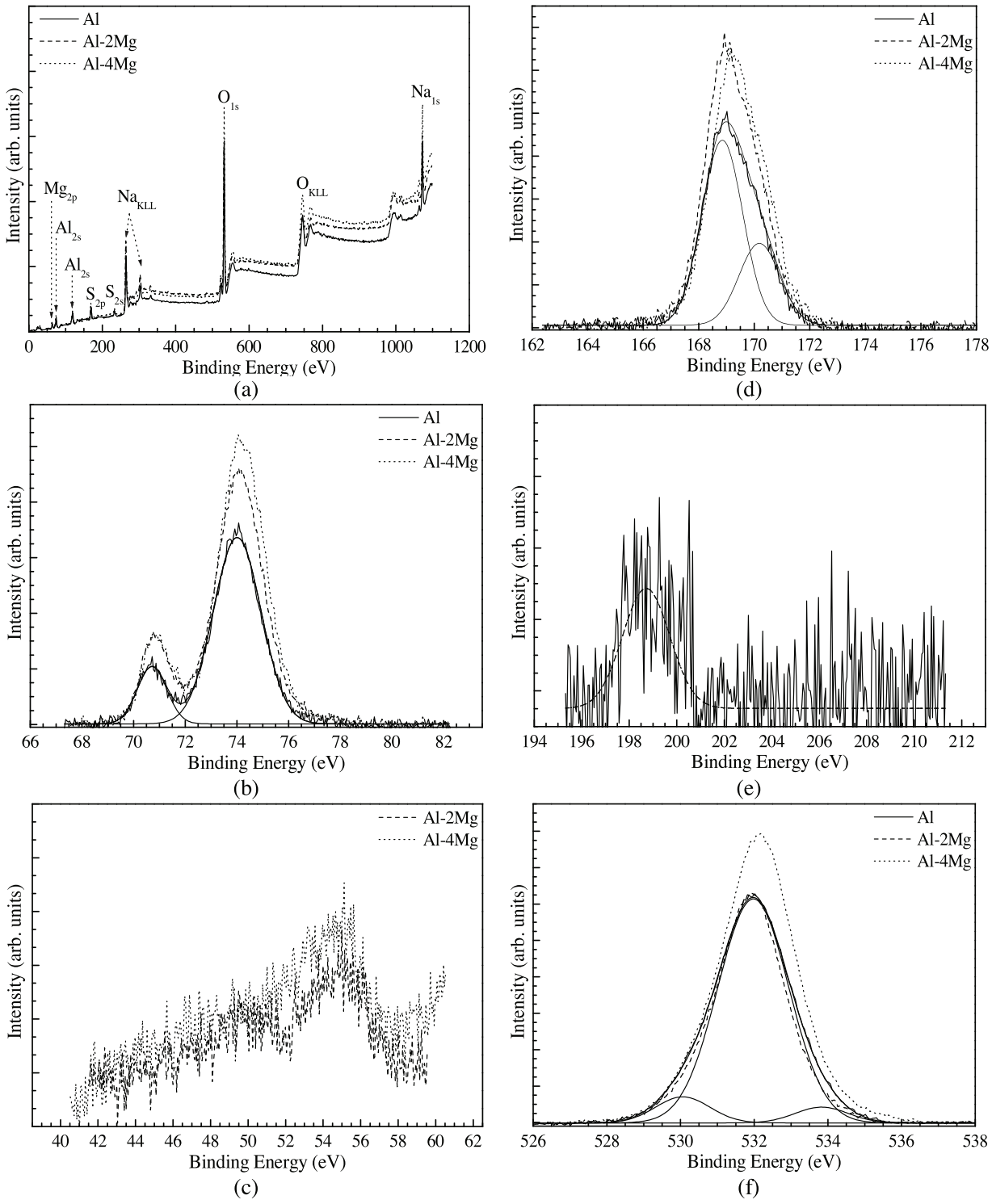

Fig. 8 – XPS peak analysis of the surface products of the alloys: (a) survey scan spectra and narrow scan spectra of (b) Al, (c) Mg, (d) S, (e) Cl, and (e) O.

(n), R_{film}, and R_{ct} as the solution resistance, CPE, and film and charge transfer resistances, respectively. The film and charge transfer resistances at medium and low frequencies can be influenced by Mg alloying [44,45]. During the fitting processes, a CPE with a phase of approximately 0.9 was used to improve the fitting quality. Fig. 6 presents the optimized R_{film} (Fig. 6(a)) and R_{ct} (Fig. 6(b)) values as a function of immersion time. These values were obtained from the Zsimpwin software by using EIS data and the equivalent circuit in Fig. 5. The fitted results indicate that both R_{film} and R_{ct} steadily increase with an increase in immersion time over 14 h. The increase in R_{film} can be attributed to the formation of a passive film on

the Al-xMg alloy surface with a mixture of $Al_2O_3/Al(OH)_3$ and $MgO/Mg(OH)_2$. This finding was confirmed through XPS, which will be discussed below. This phenomenon may be a result of the alloy dissolution processes in the investigated solution, which inhibited the penetration of aggressive ions in solution. The results also indicate that passive layer resistance significantly increases with increasing Mg content in Al-based alloys. Additionally, the R_{ct} values increase significantly with increasing Mg content, providing enhanced corrosion resistance.

Fig. 7 presents SEM images after pitting initiation during $-550\,mV_{SCE}$ application over 6 h. Pitting initiation corresponds to a sudden increase in anodic current density and the appearance of bubbles on alloy surfaces during PS measurements. The SEM results indicate that pits formed on the pure Al and Al-2Mg alloy surfaces, but no pits formed on the Al-4Mg alloy surface. Furthermore, deep and wide pits indicate that serious corrosion occurred on the pure Al surface. In contrast, corrosion developed more gradually on the Al-2Mg alloy surface. Very little corrosion occurred on the Al-4Mg alloy surface. These results correlate with the stability and durability of the passive film when the amount of Mg added to Al-based alloy increases.

Fig. 8(a) presents the peaks of Al, Mg, Na, S, Cl, O, and O-KLL in the XPS spectra of the Al-xMg alloy surfaces following 1 h of immersion in a 0.1 M Na_2SO_4 + 0.01 M NaCl solution. Additionally, the narrow spectra of the Al 2p, Mg 2p, S 2p, Cl 2p, and O 1s regions are presented in Fig. 8(b–f). The spectra of Al 2p and Mg 2p mainly highlight the existence of $Al_2O_3/Al(OH)_3$ and $MgO/Mg(OH)_2$, which promote the formation of a passive film on Al-xMg alloy surfaces. Evident formation of $Al_2O_3/Al(OH)_3$ and $MgO/Mg(OH)_2$ may be linked to the main oxide and hydroxyl groups corresponding to the oxygen signals at 530, 532, and 534 eV. The Al 2p, Mg 2p, and O 1s spectra reveal enriched products when the Mg content in the Al-based alloy increases, indicating the incorporation of Al products with Mg products. This could enhance the compactness and adhesion of the stable passive film formed on the Al-xMg alloy surfaces when considering the increases in the R_{film} and R_{ct} values shown in the EIS results above [46,47]. Furthermore, no Cl peak was observed for the Al-2Mg and Al-4Mg alloy surfaces, but Cl peak shapes were detected for the pure Al surface. Therefore, adding Mg to Al-based alloys can lead to the formation of a stable passive film that inhibits the penetration of aggressive ions in the investigated solution.

The preferential dissolution phenomenon was identified based on microgalvanic corrosion around impurity particles. When an A1 alloy containing Fe-rich impurity particles (which were verified by SEM/EDS) is immersed in the investigated solution, active Al dissolves rapidly. When active Al dissolves preferentially, impurity particles are exposed on the alloy surface. As a result, the impurity particles became cathodic to α-A1. Under severe conditions, impurity particles are left on the surface during the corrosion process based on preferential dissolution leading to pit formation, resulting in the increased depth and size of the pits shown in Fig. 7(a and b). Therefore, the relatively low pitting potential observed for the pure Al matrix is a result of the impurity particles in the Al matrix. The greater pitting potential of the Mg-containing alloys can be attributed to the decreased sizes of impurity particles in Al-Mg alloys. Because Mg dispersoids in microstructures may be located at the intersections of impurity particles and α-Al during forming processes, they may inhibit the continuity of the impurity particles in the alloy matrix, resulting in decreased impurity size with narrower and/or completely closed matrix channels in Mg-containing alloys. This could mitigate or completely prevent pitting corrosion based on the characteristics of the alloy surface. The rapid and uniform consumption of Al with Mg products results in the stable passivity of Al alloys containing Mg. Therefore, significant improvements in pitting resistance are obtained with increasing Mg content.

4. Conclusions

We successfully produced Al-xMg alloys using the hot extrusion method. Microstructure analysis confirmed a significant reduction in α-Al grain size and defects in the alloy structures. EBSD results revealed a significant reduction (~72%) in grain size from 0.63 to 0.45 μm for the pure Al and Al-4Mg alloys, respectively. Electrochemical results indicated that Al-xMg alloys provide better pitting resistance than pure Al based on high pitting potential (E_{pit}), durability of passive films, and passive and charge transfer resistances. The superior pitting resistance of Al-xMg alloys is attributed to significant changes in grain size, which enhance the formation of passive films on alloy surfaces. XPS results confirmed that the addition of Mg to Al-based alloy facilitates passive film formation based on the incorporation of Al and Mg oxides/hydroxides. Electrochemical and surface analysis results also revealed enhanced compactness and adhesion of the passive layers on alloy surfaces when the amount of Mg added to the Al-based alloys increased, indicating that the coverage of the stable passive layer determines corrosion resistance.

Conflicts of interest

The authors declare no conflicts of interest.

REFERENCES

[1] Garga P, Jamwal A, Kumar D, Sadasivunic KK, Hussaind CM, Gupt P. Advance research progresses in aluminium matrix composites: manufacturing & applications. J Mater Res Technol 2019, http://dx.doi.org/10.1016/j.jmrt.2019.06.028.
[2] Nakai M, Eto T. New aspect of development of high strength aluminum alloys for aerospace applications. Mater Sci Eng A 2000;285:62–88.
[3] Lyle JP, Granger DA, Sanders RE. Aluminum alloys. In: Ullmann's encyclopedia of industrial chemistry. Wiley-VCH; 2000.
[4] Ostermann F. TALAT — a training programme for aluminium application technologies in Europe. Mater Sci Eng A 1995;199:73–7.
[5] Pantelakis SG, Alexopoulos ND. Assessment of the ability of conventional and advanced wrought aluminum alloys for mechanical performance in light-weight applications. Mater Des 2008;29:80–91.
[6] Gupta M, Ling SJ. Microstructure and mechanical properties of hypo/hyper-eutectic Al-Si alloys synthesized using a near-net shape forming technique. J Alloys Comp 1999;287:284–94.

[7] Awotunde MA, Adegbenjo AO, Obadele BA, Okoroa M, Shongwe BM, Olubambic PA. Influence of sintering methods on themechanical properties of aluminium nanocomposites reinforced with carbonaceous compounds: a review. J Mater Res Technol 2019;8:2432–49.
[8] Noei M, Soleymanabadi H, Peyghan AA. Aluminum nitride nanotubes. Chem Pap 2017;71:881–93.
[9] Starke EA Jr, Staley JT. Application of modern aluminium alloys to aircraft. In: Lumley Roger, editor. Fundamentals of aluminium metallurgy- Production, processing and applications. Elsevier; 2011.
[10] Cuellar JS, Smit G, Plettenburg D, Zadpoor A. Additive manufacturing of non-assembly mechanisms. Addit Manuf 2018;21:150–8.
[11] Frommeyer G, Beer S, von Oldenburg K. Microstructure and mechanical properties of mechanically alloyed intermetallic Mg_2Si/Al alloys. Z Metallkd 1994;85:372–6.
[12] Tjong XSC, Ma ZY. Microstructural and mechanical characteristics of in situ metal matrix composites. Mater Sci Eng R 2000;29:49–113.
[13] Martin MA, Lu L, Gupta M. Investigation of the reactions between boron and titanium compounds with magnesium. Scr Mater 2001;45:479–86.
[14] Quevedo MC, Galicia G, Mondragon RM, Llongueras JG. Role of turbulent flow seawater in the corrosion enhancement of an Al–Zn–Mg alloy: an electrochemical impedance spectroscopy (EIS) analysis of oxygen reduction reaction (ORR). J Mater Res Technol 2018;7:149–57.
[15] Narayan S, Rajeshkannan A. Hardness, tensile and impact behaviour of hot forged aluminium metal matrix composites. J Mater Res Technol 2017;6:213–9.
[16] Ahlatci H. Wear and corrosion behaviours of extruded Al-12Si-xMg alloys. Mater Lett 2008;62:3490–2.
[17] Abdelaziz MH, Samuel AM, Doty HW, Valtierra S, Samuel FH. Effect of additives on the microstructure and tensile properties of Al–Si alloys. J Mater Res Technol 2019;8:2255–68.
[18] Chung MK, Choi YS, Kim JG, Kim YM, Lee JC. Effect of the number of ECAP pass time on the electrochemical properties of 1050 Al alloys. Mater Sci Eng A 2004;366:282–91.
[19] Uchi H, Kanno T, Alwitt RS.Electrochemical society proceedings, 99-27. 1999.
[20] Nam ND. Effect of silicon content on the electrochemical properties of Al-Si alloy. Vietnam J Sci Technol 2015;51:394–402.
[21] Cole GS, Sherman AM. Light weight materials for automotive applications. Mater Charact 1995;35:3–9.
[22] Benedyk JC. Aluminum alloys for lightweight automotivestructures A2. In: Mallick PK, editor. Materials, design andmanufacturing for lightweight vehicles. Woodhead Publishing; 2010.
[23] Khakbaz F, Kazeminezhad M. Strain rate sensitivity andfracture behaviour of severely deformed Al-Mn alloy sheets. Mater Sci Eng A 2012;532:26–30.
[24] Garner A, Tromans D. Direct observation of intergranular corrosion in Al-4 wt.% Cu alloy. Corrosion 1979;35:55–60.
[25] Urishino K, Sugimoto K. Stress-corrosion cracking of aged Al-Cu-Mg alloys in NaCl solution. Corros Sci 1979;19:225–9.
[26] Hall EO. Yield point phenomena in metals and alloys. New York: Plenum Press; 1970.
[27] Kapoor R, Chakravartty JK. Deformation behaviour of anultrafine-grained Al-Mg alloy produced by equal-channelangular pressing. Acta Mater 2007;55:5408–18.
[28] Mofid M, Loryaei E. Investigating microstructural evolution at the interface of friction stir weld and diffusion bond of Al and Mg alloys. J Mater Res Technol 2019, http://dx.doi.org/10.1016/j.jmrt.2019.06.049.
[29] Moradpour M, Khodabakhshi F, Eskandari H. Dynamic strain aging behavior of an ultra-fine grained Al-Mg alloy (AA5052) processed via classical constrained groove pressing. J Mater Res Technol 2019;8:630–43.
[30] Wang H, Wang C, Mo Y, Wang H, Xu J. Hot deformation and processing maps of Al–Zn–Mg–Cu alloy under coupling-stirring casting. J Mater Res Technol 2019;8:1224–34.
[31] Pereira PHR, Huang Yi, Langdon TG. Examining the microhardness evolution and thermal stability of an Al–Mg–Sc alloy processed by high-pressure torsion at a high temperature. J Mater Res Technol 2019;6:348–54.
[32] Tian S, Li J, Zhang J, Wulabieke Z, Lv D. Effect of Zr and Sc on microstructure and properties of 7136 aluminum alloy. J Mater Res Technol 2019, http://dx.doi.org/10.1016/j.jmrt.2019.07.022.
[33] Raynaud GM, Gomiero Ph. The potential of 5383 alloy in marine application. In: Proceedings of alumitech 97. 1997.
[34] Safari J, Chermahini MD, Akbari GH. The effect of Mg content on microstructure and mechanical properties of Al-xMg/5Al_2O_3 nanocomposite prepared by mechanical alloying. Powder Technol 2013;234:7–12.
[35] Sharma VK, Kumar V, Joshi RS. Investigation of rare earth particulate on tribological and mechanical properties of Al-6061 alloy composites for aerospace application. J Mater Res Technol 2019;8:3504–16.
[36] Bach LX, Son DL, Phong MT, Thang LV, Bian MZ, Nam ND. A study on Mg and AlN composite in microstructural and electrochemical characterizations of extruded aluminum alloy. Comp B Eng 2019;156:332–43.
[37] Qian X, Parson N, Chen XG. Effects of Mn addition and related Mn-containing dispersoids on the hot deformation behavior of 6082 aluminum alloys. Mater. Sci. Eng.: A 2019;764:138253, http://dx.doi.org/10.1016/j.msea.2019.138253.
[38] Nam ND, Dai LT, Mathesh M, Bian MZ, Thu VTH. Role of friction stir welding–traveling speed in enhancing the corrosion resistance of aluminum alloy. Mater Chem Phys 2016;173:7–11.
[39] Guan R, Tieb D, Li Z, An Y, Wang X, Li Q, Chen X. Microstructure evolution and mechanical property improvement of aluminum alloys with high magnesium content during continuous rheoextrusion. Mater Sci Eng A 2018;738:31–7.
[40] Scudino S, Sakaliyska M, Surreddi KB, Eckert J. Mechanical alloying and milling of Al-Mg alloys. J Alloys Comp 2009;483:2–7.
[41] Jeong HT, Han SH, Kim WJ. Effects of large amounts of Mg (5-13 wt.%) on hot compressive deformation behaviour and processing maps of Al-Mg alloys. J Alloys Comp 2019;788:1282–99.
[42] Searles JL, Gouma PI, Buchheit RG. Stress corrosion cracking of sensitized AA5083. Metall Mater Trans A 2001;32:2859–67.
[43] Sharma MM, Ziemian CW. Pitting and stress corrosion cracking susceptibility of nanostructured Al-Mg alloys in natural and artificial environments. J Mater Eng Perform 2008;17:870–8.
[44] Nam ND. Role of zinc in enhancing the corrosion resistance of Mg-5Ca alloys. J Electrochem Soc 2016;163:C76–84.
[45] Vuong BX, Anh HT, Nhan NT, Xuan HHM, Nguyen DC, Nam ND. Influence of the friction stir welding-traveling speed on the corrosion properties of Mg-5Al alloy. J Mater Eng Perform 2017;26:3676–85.
[46] Nam ND, Hung TV, Ngan DT, Hung NLT, Hoi TKN. Film formation in Y($4NO_2Cin$)$_3$ compound on 6061 aluminum alloy to protect against corrosion in chloride ion media. J Taiwan Inst Chem Eng 2016;67:495–504.
[47] Vuong BX, Vu NSH, Manh TD, Vaka M, Du DX, Nam ND. Role of cerium in microstructure and corrosion properties of Sn-1.0Ag solder alloys. Mater Lett 2018;228:309–13.